EAST EUROPEAN JOURNAL OF PHYSICS. **2.** 122-131 (2026)
DOI:10.26565/2312-4334-2026-2-11 ISSN 2312-4334

SUBSTITUTIONAL *Tb* INCORPORATION, $p-n$ CONDUCTIVITY TRANSITION, AND GAMMA-IRRADIATION EFFECTS ON THE THERMOELECTRIC PROPERTIES $Tb_xSn_{1-x}Se$ SOLID SOLUTIONS

T.A. Jafarov[1], A.M. Allahverdiyev[1], G.A. Garashova[1], Kh.A. Adgezalova[1], O.M. Gasanov[1], I.M. Mammadov[1], J.I. Huseynov[1]*, I.I. Abbasov[2], V.I. Hajiyeva[3]
[1]*Azerbaijan State Pedagogical University, AZ-1000, Baku, Uz. Hajibeyli Str. 68, Azerbaijan*
[2]*Azerbaijan State Oil and Industry University,* Az-1010, *Baku, Azadlıq Avenue 20, Azerbaijan*
[3]*Nakhchivan State University, AZ7000, Nakhchivan city, Istiglal Street 85, Azerbaijan*
**Corresponding Author email: jahangirhuseynov1958@gmail.com*
Received March 2, 2026; revised April 21, 2026; in final form April 30, 2026; accepted May 13, 2026

The physicochemical and thermoelectric properties of $Tb_xSn_{1-x}Se$ $(0 \le x \le 0.05)$ solid solutions were systematically investigated with emphasis on composition-driven carrier-type transition and $\gamma-$irradiation effects. Differential thermal analysis reveals a monotonic decrease in melting temperature and enthalpy with increasing Tb content, indicating lattice distortion and reduced thermal stability due to the substitutional incorporation of Tb^{3+} at Sn^{2+} sites. $X-$ray diffraction confirms single-phase orthorhombic $(Pnma)$ structure without secondary phases, while EDX analysis verifies successful Tb incorporation. A composition-induced $p-n$ transition occurs within a narrow concentration range, accompanied by a significant modification of the Seebeck coefficient. $\gamma-$irradiation (up to $4-6.5\ Mrad$) significantly affects the Seebeck coefficient in the low-temperature region $(80-300\ K)$, with a nonlinear dose dependence that can be approximated by a quadratic function. At elevated temperatures $(T \ge 500\ K)$, the thermoelectric response exhibits notable radiation stability. The obtained results clearly indicate that Tb doping facilitates a controllable modulation of charge carrier transport properties while preserving the structural integrity and thermal stability of the material at elevated temperatures. These findings underscore the strong potential of $Tb-$doped systems for advanced thermoelectric applications, particularly under radiation-exposed operating conditions.
Keywords: *Solid solutions; Substitutional doping; $p-n$ conductivity transition; Seebeck coefficient; Gamma irradiation; Radiation-modified thermoelectric transport*
PACS:71.20.Nr, 72.20.Pa, 61.72.-y

1. INTRODUCTION

Layered crystals are a class of materials with a unique structure, where atomic layers are held together by weak van der Waals forces. These materials occupy an intermediate position between molecular and nanoscale structures. They possess unique physicochemical properties, making them promising nanomaterials [1, 2]. The effects observed when forming low-dimensional structures with subnanometer-scale constraints in binary semiconductor compounds are related to the nature of the chemical bond and the crystal structure of the bulk phases. The relationship between the structure and properties of three-dimensional crystals and low-dimensional structures is examined using three classes of compounds– $A^{IV}B^{VI}, A^{III}B^{VI}, A_2^VB_3^{VI}$[3, 4].

Among $IV-VI$ binary compounds, including $GeS, GeSe, SnS,$ and $SnSe,$ a pronounced anisotropic layered crystal structure is observed. Within each layer, atoms are strongly bonded via covalent interactions, whereas adjacent layers are held together by relatively weak van der Waals forces. Owing to these weak interlayer interactions, such crystals can be readily exfoliated into atomically thin sheets, analogous to graphene [5,6]. This structural feature provides significant potential for applications in nanotechnology and two-dimensional (2D) electronics. Furthermore, the layered architecture inherently reduces lattice thermal conductivity, which is advantageous for thermoelectric performance. The pronounced anisotropy in their electronic properties can further enhance the efficiency of heat-to-electric energy conversion [7].

The incorporation of rare-earth elements (REEs) into tin monoselenide induces a range of physical phenomena governed by the formation, energetics, and interactions of intrinsic and impurity-related defects. In semiconductor matrices, REE impurities exhibit distinctive behavior, notably their limited solid solubility and their pronounced gettering capability, whereby they effectively reduce the concentrations of residual impurities and defect states, leading to a significant purification of the host material [8, 9].

Materials derived from rare earth elements (REEs) are extensively employed in the fabrication of advanced energy conversion systems, a wide range of thermistor devices, and functional materials exhibiting enhanced resistance to radiation, mechanical pressure, and environmental humidity. Doping $SnSe$ with rare earth metals is an effective method for controlling its electrophysical properties. It enables optimization of thermoelectric characteristics, reduction of

Cite as: T.A. Jafarov, A.M. Allahverdiyev, G.A. Garashova, Kh.A. Adgezalova, O.M. Gasanov, I.M. Mammadov, J.I. Huseynov, I.I. Abbasov, V.I. Hajiyeva, East Eur. J. Phys. 2, 122 (2026), https://doi.org/10.26565/2312-4334-2026-2-11

thermal conductivity, increase in electrical conductivity, and improved material stability, making *SnSe* even more promising for use in thermoelectrics and electronics [10, 11].

The thermoelectric performance of *SnSe* – based semiconductors is highly sensitive to compositional modifications and external perturbations that govern charge-carrier transport and phonon scattering [12]. In particular, substitutional incorporation of rare-earth elements such as Tb introduces localized electronic states, alters carrier concentration, and may induce a p–n conductivity transition, leading to substantial changes in transport properties.

Gamma irradiation provides an additional degree of control via defect engineering, generating point defects and defect complexes that modify carrier scattering, relaxation processes, and energy-filtering effects [13]. As thermoelectric coefficients are strongly dependent on the energy-dependent relaxation of charge carriers, their temperature behavior provides a sensitive probe of the underlying scattering mechanisms and the evolution of the electronic structure [14].

In this context, $Sn_{1-x}Tb_xSe$ solid solutions represent a promising system for investigating the combined effects of substitutional doping and radiation-induced defects. Such interplay is critical for understanding transport phenomena and optimizing thermoelectric performance in multicomponent chalcogenides.

In this work, $Sn_{1-x}Tb_xSe$ compounds were synthesized, and their thermoelectric properties were systematically studied as functions of composition, temperature, and gamma irradiation dose. The results provide insight into charge-transport mechanisms and demonstrate viable pathways for tailoring thermoelectric materials through rare-earth doping and irradiation-induced defect engineering.

2. EXPERIMENTAL PART

For the synthesis of SnSe–TbSe alloys, high-purity (4N–5N grade) tin, selenium, and gadolinium were used (tin ≥ 99.99%, selenium ≥ 99.999%, terbium 99.98%). The synthesis was carried out in evacuated quartz ampoules at a pressure of $0.1333\ Pa$using a two-step direct fusion method. In the first stage, the ampoule with the material was heated at a rate of $4-5\ degrees$ per minute to the melting point of selenium and held at this temperature for $3-4\ hours$. Then, the temperature was gradually increased to $950-1000°C$ (depending on the composition) and maintained for $8-9\ hours$.

To perform comprehensive physicochemical analysis and electrophysical studies, the obtained samples were annealed for $140-210\ hours$ (depending on the composition). The duration of the annealing increased with the gadolinium content. The homogenizing annealing of the obtained single-phase samples was carried out in a spectrally pure argon atmosphere.

The interaction in the $SnSe-TbSe$ system was studied using differential thermal analysis (DTA), X-ray phase analysis (XRD), microstructural analysis (MSA), as well as by measuring microhardness and determining density. To determine the thermal effects of the obtained samples and phase transitions, DTA was performed using a PerkinElmer Simultaneous Thermal Analyzer STA 6000 (USA). Nitrogen was used as the working gas with a flow rate of $20\ ml/sec$; the sample was heated to the melting temperature at a rate of$5\ °C/min$.

X-ray structural analysis was performed using a Rigaku Corporation Miniflex $X-ray$ diffractometer at a voltage of $30\ kV$, current of $10\ mA$, and $CuK\alpha$ radiation ($\lambda = 1.5406$ Å). Diffraction peaks were recorded at a 2θdeviation angle in the range from 0 to 80°. To study the morphology and microcomposition of the sample surfaces, a Japanese JEOL JSM6610-LV scanning electron microscope was used.

The samples were irradiated using an RHUND-20000 continuous-wave radiation chemical unit with a photon energy of 1.25 MeV and doses in the range $D_\gamma = 0-6.5\ Mrad$. The radiation flux density was $1.4\cdot10^{11}\ \text{photons}/c\cdot cm^2$. One day after irradiation, the thermoelectric power was measured using the steady-state compensation method in the temperature range of 80-900 K [15]. While a constant electric current was applied along [100], the measurement error for the thermo-EMF was approximately ~4.6%.

3. RESULTS AND DISCUSSION

3.1. Physicochemical Analysis

Figure 1 presents the differential thermal analysis (DTA) curves of $Tb_xSn_{1-x}Se$ solid solutions in the composition range $x = 0-0.04$. For all samples, a pronounced endothermic peak is observed in the high-temperature region, corresponding to the solid–liquid phase transition (melting).

The melting temperature was determined from the peak maximum, i.e., $T_m(x) = T_{peak}$. The main thermal parameters, including the onset ($\boldsymbol{T_{onset}}$), peak ($\boldsymbol{T_{peak}}$), and endset ($\boldsymbol{T_{end}}$) temperatures, peak height (ΔDTA), full width at half maximum (FWHM), and transition enthalpy (ΔH), were extracted from the DTA curves and are summarized in Table 1. As seen, both $\boldsymbol{T_{onset}}$, and T_m systematically shift toward lower temperatures with increasing Tb content. Specifically, the melting temperature decreases from approximately $1117\ K$ for pristine $SnSe$ to about $1076\ K$ for $x = 0.04$.

This reduction in melting temperature can be attributed to the incorporation of Tb ions into the $SnSe$ lattice, leading to local lattice distortions, reduced average bond strength, and decreased thermal stability. These results indicate the formation of a substitutional solid solution over the composition range studied.

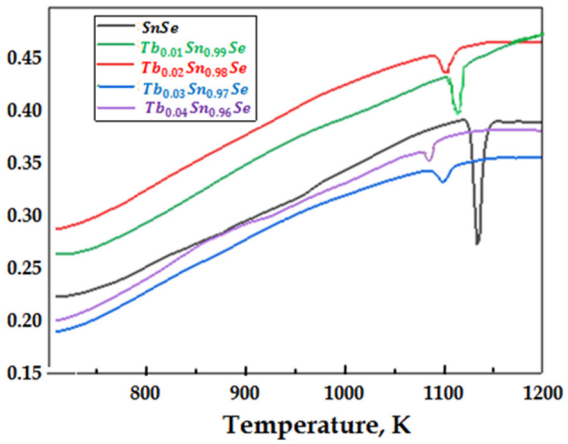

Figure 1. DTA curves of system alloys $Tb_xSn_{1-x}Se$

A concurrent decrease in peak height (ΔDTA) and increase in FWHM with increasing Tb concentration suggest that the phase transition becomes more diffuse and occurs over a broader temperature interval. This behavior reflects increasing structural disorder and compositional inhomogeneity induced by Tb doping. The monotonic decrease in the transition enthalpy ΔH with increasing Tb content indicates that the energy required for the phase transition decreases with doping. This behavior suggests a weakening of long-range structural order and a decrease in lattice cohesion.

Table 1. Thermal parameters of $Tb_xSn_{1-x}Se$ solid solutions derived from DTA curves

Composition	T_{onset} (K)	T_m (K)	T_{end} **(K)**	**Peak height, ΔDTA**$(\mu V/mg)$	**FWHM (K)**	**Transition enthalpy,** ΔH (J/g)
SnSe	*≈1108*	*≈1117*	*≈1135*	*≈0.09*	*≈18*	**≈ 10.2**
$Tb_{0.01}Sn_{0.99}Se$	*≈1092*	*≈1103*	*≈1126*	*≈0.075*	*≈22*	≈ 9.0
$Tb_{0.02}Sn_{0.98}Se$	*≈1078*	*≈1091*	*≈1116*	*≈0.065*	*≈26*	≈ 7.8
$Tb_{0.03}Sn_{0.97}Se$	*≈1069*	*≈1082*	*≈1107*	*≈0.055*	*≈30*	≈ 6.3
$Tb_{0.04}Sn_{0.96}Se$	*≈1062*	*≈1076*	*≈1102*	*≈0.050*	*≈34*	**≈ 5.2**

Furthermore, the absence of additional peaks in the DTA curves indicates that no secondary Tb −based phases are formed, confirming that Tb is incorporated homogeneously into the $SnSe$ matrix and that the system remains phase-stable within the investigated composition range. In summary, DTA analysis demonstrates that Tb doping significantly reduces both the melting temperature and transition enthalpy $SnSe$ −based solid solutions [16].

These trends are consistent with our previous studies on $SnSe$ doped with other rare-earth elements (RE), where a similar reduction in melting temperature and transition enthalpy was observed with increasing dopant concentration. In all cases, the incorporation of RE ions into the $SnSe$ lattice leads to lattice distortions and weakening of interatomic bonding, resulting in reduced thermal stability. However, while the qualitative behavior remains the same, quantitative differences in the magnitudes of these effects vary with the specific rare-earth element. This can be attributed to differences in ionic radii associated with the lanthanide contraction and the degree of $4f$ −electron shell filling. Therefore, Tb doping follows the general trend characteristic of RE-doped $SnSe$ systems, while exhibiting element-specific variations in thermal parameters.

X-ray diffraction patterns for all compositions exhibit reflections consistent with orthorhombic $SnSe$ $(Pnma)$, with no detectable impurity phases. The principal diffraction peaks display slight but systematic 2θ shifts with increasing Tb concentration, consistent with lattice distortion induced by partial substitution of Sn^{2+} by Tb^{3+} ions. No reflections attributable to oxide or secondary chalcogenide phases are observed within the detection limit, confirming phase purity and controlled synthesis conditions [17].

Similar behavior has been reported in our previous studies on $SnSe$ doped with other rare-earth elements, where systematic peak shifts and lattice parameter changes were also observed. This confirms that the substitutional incorporation mechanism is common for RE dopants in $SnSe$. Nevertheless, slight differences in the extent of lattice expansion can be attributed to variations in ionic radii and electronic structure among different lanthanides.

Analysis of X −ray diffraction data indicates that the introduction of Terbium selenides leads to an increase in the lattice parameters of $SnSe$ as the Tb concentration increases. Furthermore, intense charge carrier scattering is observed due to lattice "distortions," which aligns with the thermal conductivity data of these alloys [18]. The slight shift of diffraction lines in the X-ray diffraction patterns in the $0-5\ mol\%$ range, the observed increase in elementary lattice parameters, good agreement with the partial replacement of Sn atoms by Tb atoms with larger radii, and compliance with Vegard's law suggest the formation of substitutional solid solutions based on $SnSe$ [19].

The surface morphology of $Tb_{0.02}Sn_{0.98}Se$ crystals was systematically investigated using scanning electron microscopy (SEM) combined with quantitative surface topography analysis. The results are summarized in Fig. 2.

The two-dimensional surface map (Fig. 2a) reveals a high degree of spatial uniformity, with no visible macroscopic defects such as cracks, voids, or inclusions. The corresponding three-dimensional reconstruction (Fig. 2b) shows that the surface is composed of uniformly distributed nanoscale protrusions and depressions, forming a homogeneous microrelief.

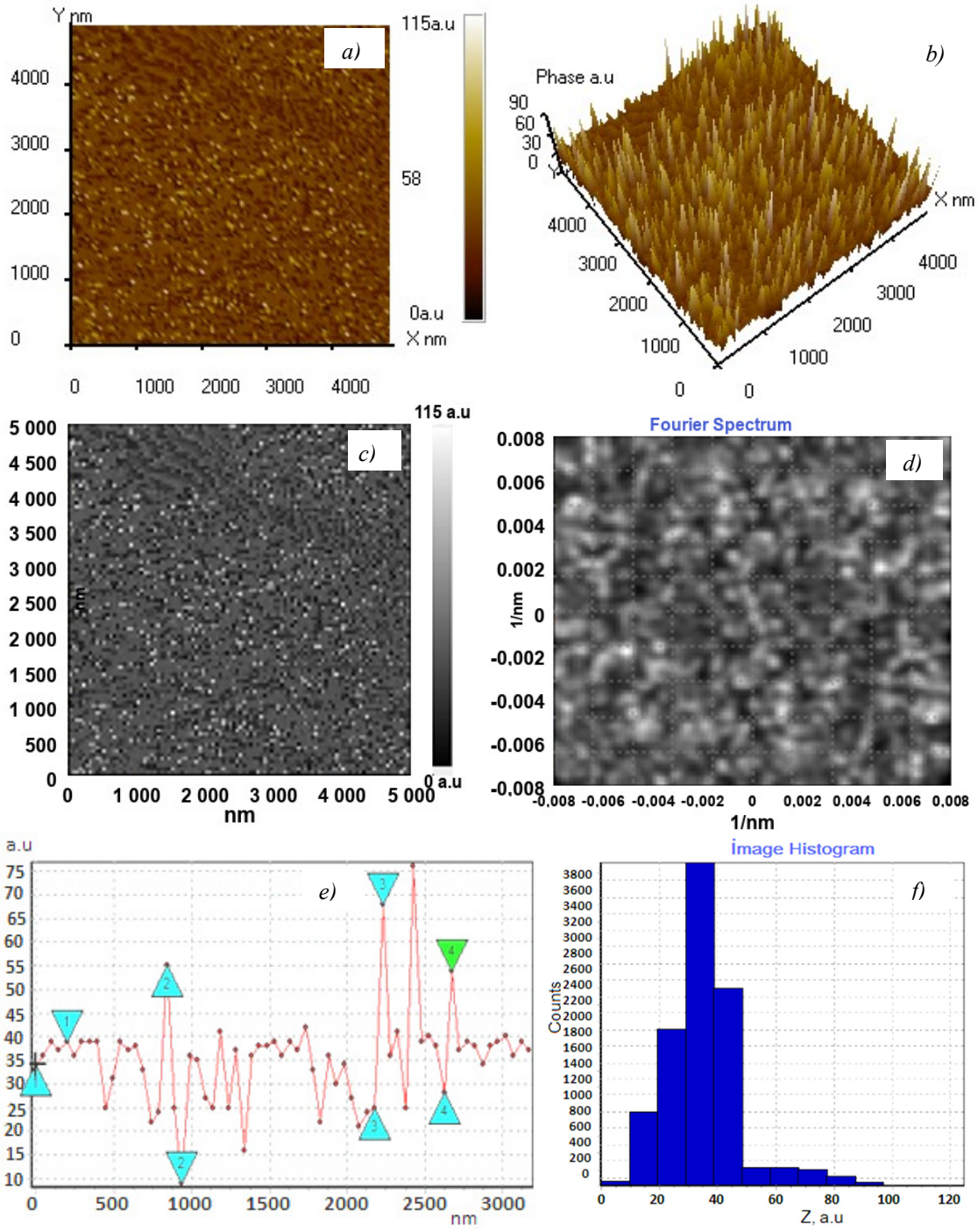

Figure 2. Surface morphology and statistical analysis of $Tb_{0.02}Sn_{0.98}Se$ crystals: *a)* 2D topographic image of the surface; *b)* 3D surface reconstruction showing height variations; *c)* SEM image illustrating the microstructure and grain distribution; *d)* Fourier spectrum of the surface, indicating spatial frequency distribution; *e)* line profile of surface roughness along a selected scan; f) height distribution histogram of the surface

Quantitative roughness analysis was carried out using the height profile (Fig. 2e) and statistical distribution (Fig. 2f). The extracted roughness parameters are: average roughness $R_a \approx 5-15$ nm, root-mean-square roughness $R_q \approx 7\text{-}20\,nm$, and maximum peak-to-valley height $R_Z \approx 30-60\,nm$. These relatively low roughness values indicate a smooth surface at the nanometer scale, which is typically associated with high crystalline quality and controlled growth conditions.

AFM and SEM analyses demonstrate that the Tb dopant is highly homogeneously distributed along the surface, with no signs of phase separation or clustering observed. The diffuse nature of the Fourier spectrum and the Gaussian-type statistics of the surface height distribution are in good agreement with the substitution of Tb atoms mainly for Sn positions in the crystal lattice.

Overall, the combined morphological and statistical analyses demonstrate that $Tb_xSn_{1-x}Se$ crystals possess a nanostructured yet highly homogeneous surface. This structural quality is expected to play a crucial role in determining charge carrier transport and phonon scattering mechanisms, making these materials promising candidates for thermoelectric applications.

The energy-dispersive X-ray (EDX/EDR) spectrum of the $Tb_xSn_{1-x}Se$ sample (x = 0.01) shows distinct characteristic peaks of Sn, Se, and Tb, confirming the successful incorporation of terbium into the crystal lattice (Fig. 3). Under high-energy electron irradiation, inner-shell ionization (K, L, M) leads to electronic transitions accompanied by the emission of characteristic X-rays. For Sn, the dominant L-series lines (SnL_α~3.44 keV and L_β ~3.67 keV) are observed, while Se exhibits $L_\alpha(\sim 1.38\ keV)$, $L_\beta(\sim 1.43\ keV)$, and $K_\alpha(\sim 11.22\ keV)$ lines, confirming the preservation of the $SnSe$ matrix phase. The presence of Tb is verified by both $M-$series (M_α~1.24 keV, M_β ~1.30 keV) and $L-$series (L_α~6.27 keV, L_β ~6.68 keV) emission lines. The multiplicity of Tb peaks reflect its complex electronic structure and support its partial substitution at Sn lattice sites [20]. Overall, the EDX results confirm Tbincorporation into the primary phase without evidence of secondary phase formation.

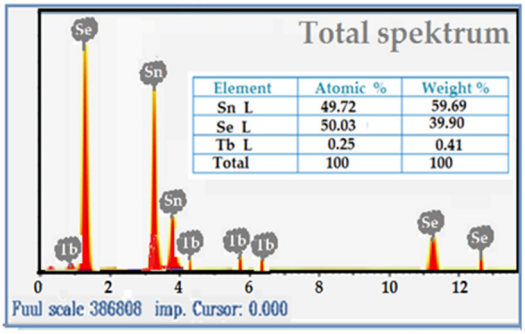

Figure 3.X-ray microanalysis of the crystal surface$Tb_xSn_{1-x}Se$:2- x=0,005

Collectively, thermal, structural, compositional, and morphological analyses consistently demonstrate that low-level Tb incorporation in $SnSe$leads to substitutional solid-solution formation, slight lattice distortion, reduced thermal stability, and preserved phase purity without secondary-phase formation

3.2. Composition-Driven p–n Transition and γ-Irradiation Effects on the Seebeck Coefficient of $Tb_xSn_{1-x}Se$ Solid Solutions

In the study reported in [21], the kinetic and transport parameters of $Tb_xSn_{1-x}Se$ solid solutions ($0 \le x \le 0.05$), grown by the Bridgman technique, were systematically investigated at $T = 300\ K$. It was established that terbium doping exerts a pronounced influence on the electrical conductivity, Hall coefficient, thermoelectric power, thermal conductivity, as well as on the charge carrier concentration and mobility. With increasing Tb content in the $SnSe-$based solid solutions, the Seebeck coefficient S initially decreases sharply within the composition range $0 \le x \le 0.002\ mol.\%$ (from $+420$to $+128\ \mu V/K$). This behavior is attributed to the donor effect associated with the substitution of Sn^{2+} ions by Tb^{3+} ions, which leads to electron generation and enhanced carrier scattering due to lattice distortion and local symmetry breaking. Within the narrow concentration interval $0.002 < x < 0.0025\ mol.\%$, a sign inversion of the Seebeck coefficient occurs (down to $-325\ \mu V/K$), indicating a transition from $p-$type to $n-$type conductivity. This inversion reflects a shift of the Fermi level toward the conduction band and the formation of localized donor states introduced by Tb impurities. For $0.0025 < x < 0.015\ mol.\%$, negative values of S become stabilized, confirming the establishment of electron-dominated (n-type) transport and partial saturation of donor states. At higher Tb concentrations ($0.02 < x < 0.05\ mol.\%$), a gradual reduction in the absolute value of the Seebeck coefficient is observed. This tendency is associated with an increase in free electron concentration, a corresponding decrease in the chemical potential gradient, and possible carrier localization effects arising from $Tb-Tb$ interactions and partial ordering within the defect sublattice of the crystal structure.

The effect of γ-irradiation on the thermoelectric properties of $Tb_xSn_{1-x}Se$ solid solutions was investigated at room temperature within an absorbed dose range of 0–6.5 Mrad (Fig. 4. *a)*). The Seebeck coefficient evolution strongly depends on the conductivity type. For $p-$type compositions (x ≤ 0.001), a non-monotonic $S(D)$ dependence is observed: the Seebeck coefficient initially increases with dose, reaches a maximum, and then decreases. For $x = 0, S$ rises from $\approx +420\ \mu V/K$ to $\approx +442\ \mu V/K$at $D \approx 5\ Mrad$, followed by a slight reduction. A similar trend is found for $x = 0.001$ (from $\approx +275$to $\approx +285\ \mu V/K$). This behavior is attributed to radiation-induced donor-type point defects, which enhance compensation of hole carriers. At higher doses, defect saturation and enhanced carrier scattering lead to a decrease in S. Such behavior is characteristic of radiation-modified $p-$type $SnSe$.

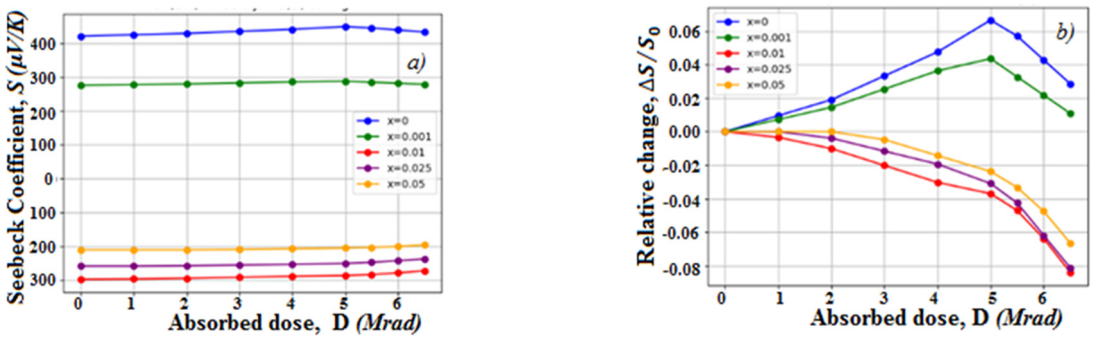

Figure 4. Dependence of the Seebeck coefficient a) and its relative change b) on the absorbed dose

For $n-$type samples ($x \geq 0.01$), the magnitude of the Seebeck coefficient decreases monotonically with increasing dose. Specifically, S changes from ≈ -297 to $-272\,\mu V/K$ ($x = 0.01$), from ≈ -258 to $-237\,\mu V/K$ ($x = 0.025$), and from $\approx -210\,to-196\,\mu V/K$ ($x = 0.05$). The reduction of |S| is associated with increased electron concentration and enhanced scattering due to radiation-induced defects. The conductivity type remains unchanged throughout the entire dose range, and no $p-n$ conversion is observed [22].

The analysis of the relative change, $\Delta S/S_0 = (S(D) - S_0)/S_0$, shows that for $p-$type samples it is positive and reaches $\sim 4-5\%$ with a subsequent tendency toward saturation (Fig. 4.*b*)), whereas for n-type samples it takes negative values (down to $-7-8\%$). The $\Delta S/S_0(D)$ dependence is nonlinear and can be satisfactorily approximated by a quadratic function of the form $\Delta S/S_0(D) \approx aD^2 + bD + c$. This approach accounts for both the initial defect-induced compensation contribution and the saturation and enhanced scattering effects at higher doses, thereby providing an analytical framework for describing and predicting the radiation-induced thermoelectric behavior of $Tb_xSn_{1-x}Se$ solid solutions.

3.3. Diffusion, phonon-drag, and bipolar contributions to the Seebeck coefficient in $Tb_xSn_{1-x}Se$ solid solutions

The temperature dependence of the Seebeck coefficient for $Tb_xSn_{1-x}Se$ solid solutions with different terbium concentrations is presented in Fig. 5. The obtained results demonstrate that both compositional variation and temperature exert a pronounced influence on the charge transport mechanisms and electronic structure of the system.

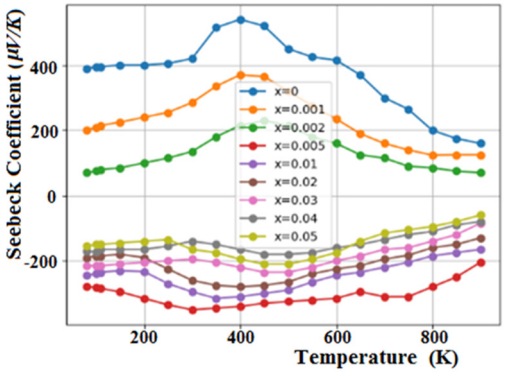

Figure 5. Temperature dependence of the Seebeck coefficient in $Tb_xSn_{1-x}Se$system alloys

In general, the total Seebeck coefficient can be expressed as the superposition of diffusion and phonon-drag contributions [24]:

$$S = S_{diff} + S_{ph}$$

where $S_{diff}-$ denotes the carrier diffusion component and $S_{ph}-$ corresponds to the phonon-drag contribution.

In the intermediate temperature range, the phonon-drag term typically attains a maximum due to efficient momentum transfer from nonequilibrium phonons to charge carriers [25]. However, at elevated temperatures, intensified phonon–phonon scattering significantly suppresses this effect, resulting in a gradual decrease of the total Seebeck coefficient. The systematic decrease in S observed above 400 K across all p-type samples (Fig. 5) is fully consistent with this mechanism.

For the undoped sample (x = 0), the Seebeck coefficient reaches a maximum of approximately 540 μV/K over the temperature range 350–400 K. The initial increase in S with temperature is primarily attributed to the enhancement of the phonon-drag mechanism, which dominates the diffusion contribution in this range.

As shown in Fig. 5, compositions with $x = 0, 0.001$, and 0.002 exhibit positive Seebeck coefficients over the entire investigated temperature interval, indicating hole-dominated transport ($p-$type conductivity). In contrast, for

$x \geq 0.005$, the Seebeck coefficient becomes negative (S<0), evidencing a transition to electron-dominated ($n-$type) conductivity. This behavior indicates that beyond a critical Tb concentration, a compensation mechanism is activated, leading to a shift of the Fermi level toward the conduction band and ultimately altering the dominant carrier type.

For semiconductors, the diffusion component of the Seebeck coefficient can be described by [12]:

$$S_{diff} = \frac{k_B}{e}\left(\frac{r+2}{r+1} - \frac{E_F - E_C}{k_B T}\right)$$

where $k_B -$ is the Boltzmann constant, $e -$is the elementary charge, $E_F -$ is the Fermi level, $E_C -$ is the conduction band minimum, and $r -$ is the scattering parameter that characterizes the dominant carrier-scattering mechanism.

According to this relation, variations in the Fermi level position directly affect both the magnitude and the sign of the Seebeck coefficient. Therefore, the experimentally observed sign inversion is in good agreement with theoretical predictions.

With increasing Tb content, a systematic decrease in the absolute value of the Seebeck coefficient is observed. This trend is directly associated with the increase in charge carrier concentration induced by doping. For non-degenerate semiconductors, the Seebeck coefficient approximately follows:

$$S \sim \frac{k_B}{e} ln\left(\frac{N_v}{n}\right)$$

where$n$ is the carrier concentration and $N_v -$ is the effective density of states in the valence band.

As the Tb concentration increases, the carrier concentration rises, leading to a reduction in S. The experimentally observed decrease in the maximum Seebeck values for $x = 0.001$ and 0.002 quantitatively supports this theoretical dependence.

For samples with $x \geq 0.005$, the Seebeck coefficient becomes negative and exhibits a pronounced extremum within the $250 - 350\ K$ temperature interval. The subsequent reduction of $|\ S\ |$ at higher temperatures can be attributed to the onset of bipolar conduction. As temperature increases, intrinsic carrier excitation generates electron–hole pairs, thereby reducing the net thermoelectric response. In the bipolar regime, the effective Seebeck coefficient can be expressed as [26]:

$$S_{bipolar} \propto \left(\frac{\sigma_n S_n + \sigma_p S_p}{\sigma_n + \sigma_p}\right)$$

where $\sigma_n -$ and $\sigma_p -$ represent the electrical conductivities of electrons and holes, respectively, while $S_n -$ and $S_p -$ denote their partial Seebeck coefficients.

The simultaneous contribution of both carrier types leads to partial compensation, which decreases the overall Seebeck coefficient at elevated temperatures.

In summary, the analysis of Fig. 5 reveals that:

– Tb doping induces a conductivity-type transition from $p -$type to $n -$type behavior.

– The maximum of the Seebeck coefficient is located within the $300 - 400\ K$ temperature range.

– Increasing Tb concentration reduces the magnitude of S due to enhanced carrier concentration and the corresponding Fermi level shift.

– The high-temperature decrease in S is primarily governed by bipolar diffusion effects.

These findings demonstrate that Tb incorporation effectively tunes the electronic structure and carrier transport parameters of the $Tb_xSn_{1-x}Se$ system, highlighting its potential for thermoelectric applications in the intermediate temperature range [27].

3.4. Effect of Gamma Irradiation on the Seebeck Coefficient of $Tb_xSn_{1-x}Se$ Alloys

The Seebeck coefficient (S) of $Tb_xSn_{1-x}Se$ alloys $(x = 0, 0.001, 0.005, 0.01, 0.05)$ was measured in the temperature range $80 - 900\ K$ before and after $\gamma -$irradiation with an absorbed dose of 4 $Mrad$. The obtained results reveal a pronounced temperature- and composition-dependent radiation effect (Fig. 6).

In the low-temperature region$(80 - 300\ K)$, $\gamma -$irradiation significantly modifies the Seebeck coefficient for all investigated compositions. For the undoped sample $(x = 0)$, S increases over the entire range. For example, at $80\ K$, S rises from 390 to 475 $\mu V/K$ $(\Delta S \approx +85\ \mu V/K)$, corresponding to a relative increase of about 22%. A similar trend is observed at $100\ K$ $(393 \rightarrow 471\ \mu V/K)$. Such behavior indicates a substantial modification of charge carrier parameters due to radiation-induced defect formation [28].

For weakly doped samples $(x = 0.001)$, the Seebeck coefficient also increases after irradiation, particularly below $200\ K$, where the relative change reaches $10 - 15\%$. This behavior can be attributed to radiation-induced trapping centers that reduce the effective carrier concentration and modify the energy dependence of electrical conductivity.

For compositions with $x = 0.005$ and characterized by negative Seebeck coefficients ($n -$type conductivity), irradiation leads to an increase in the absolute value $|S|$ in the low-temperature region. For instance, for $x = 0.005$ at $80\ K$, S changes from -280 to $-316\ \mu V/K$. This enhancement in $|S|$ suggests a decrease in electron concentration

and/or increased carrier scattering caused by radiation-induced structural disorder. Although a sign anomaly is observed at $100\ K$ for $x = 0.05$, the overall temperature dependence preserves the n −type character [29].

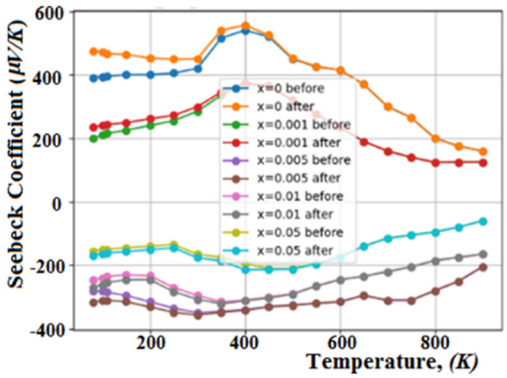

Figure 6. Temperature dependence of the Seebeck coefficient before and after irradiation in $Tb_xSn_{1-x}Se$ system alloys

In the intermediate temperature range$(300 - 500\ K)$, the radiation effect gradually weakens. For $x = 0$, the maximum difference is observed near $350\ K$ $(515 \rightarrow 540\ \mu V/K)$, but the relative variation decreases with increasing temperature. A similar tendency is found for other compositions. This behavior indicates that at elevated temperatures phonon scattering becomes dominant over defect scattering, partially compensating the radiation-induced modifications.

At high temperatures$(T \geq 500\ K)$, the Seebeck coefficients of irradiated and non-irradiated samples practically coincide for all investigated compositions:

$$S_{befor}(T) \approx S_{after}(T), T > 500K$$

This result demonstrates that thermally activated carriers and intrinsic conduction mechanisms dominate transport properties in this temperature range, while the contribution of radiation-induced defects becomes negligible. Therefore, the $Tb_xSn_{1-x}Se$ system exhibits considerable radiation stability of thermoelectric properties at high temperatures.

In addition, the convergence of the Seebeck coefficients at high temperatures may also indicate the partial thermal annealing or reconfiguration of radiation-induced defects during the measurement process. At elevated temperatures, increased atomic mobility can lead to a reduction in the concentration or activity of defect centers responsible for carrier scattering and trapping. As a result, the influence of γ-induced defects becomes progressively weaker, and the transport properties are governed predominantly by intrinsic mechanisms. Although repeated measurements after high-temperature cycling were not performed in the present study, the observed behavior is consistent with the expected thermal stability and defect dynamics in narrow-gap thermoelectric semiconductors.

The observed changes in S can be interpreted within the framework of the Mott relation [30]:

$$S = \frac{\pi^2 k_B^2 T}{3e} \frac{dln\sigma(E)}{dE}_{|\ E=E_F}$$

which shows that the Seebeck coefficient depends on the energy derivative of electrical conductivity near the Fermi level. Gamma irradiation modifies the density of states and scattering mechanisms through defect formation, thereby altering the energy dependence of $\sigma(E)$. The most pronounced effects occur at low temperatures, where transport is highly sensitive to impurity and defect scattering. With increasing temperature, intrinsic carrier excitation reduces the relative impact of radiation-induced defects.

Overall, γ −irradiation with a dose of 4 $Mrad$ significantly affects the Seebeck coefficient of$Tb_xSn_{1-x}Se$ alloys in the low-temperature region $(80 - 300\ K)$, while the effect becomes negligible above $600\ K$. The magnitude of the radiation response depends on terbium concentration and conduction type, being more pronounced for low Tb content and in samples near the compensation regime.

4. CONCLUSIONS

A comprehensive investigation of the physicochemical, structural, compositional, and thermoelectric properties of $Tb_xSn_{1-x}Se$ $(0 \leq x \leq 0.05)$ solid solutions has been performed, including the influence of γ −irradiation on the Seebeck coefficient over a wide temperature range.

Thermal analysis demonstrates that terbium incorporation leads to a monotonic decrease in melting temperature, reduced relative melting enthalpy, and peak broadening, indicating lattice softening and increased structural disorder. X-ray diffraction confirms the preservation of the orthorhombic $SnSe$ $(Pnma)$ structure without detectable secondary phases, while systematic peak shifts evidence substitutional incorporation of Tb^{3+} at Sn^{2+} lattice sites. Surface morphology analysis reveals a homogeneous nanostructured relief that may enhance phonon and carrier scattering. EDX spectroscopy further verifies the successful Tb incorporation into the primary phase, confirming the formation of a substitutional solid solution with preserved phase purity.

Compositionally driven transport measurements reveal a Tb −induced $p-n$ conductivity transition. At low Tb concentrations, donor states introduced by Tb^{3+} ions compensate holes and shift the Fermi level toward the conduction band. A sign inversion of the Seebeck coefficient occurs within a narrow composition interval, confirming the transition from p −type to n −type conduction. Increasing Tb content systematically reduces the magnitude of the Seebeck coefficient due to enhanced carrier concentration and Fermi level shift, consistent with diffusion thermo power models. Temperature-dependent measurements indicate that the total Seebeck coefficient arises from diffusion and phonon-drag contributions at intermediate temperatures $(300-400\ K)$, while bipolar conduction effects dominate at elevated temperatures.

The effect of γ-irradiation (up to $4-6.5\ Mrad$) strongly depends on conductivity type and temperature. In the low-temperature region $(80-300\ K)$, irradiation significantly modifies the Seebeck coefficient: p −type samples exhibit a non-monotonic increase associated with radiation-induced donor-like defects and carrier compensation, whereas n-type samples show a monotonic reduction in $|S|$ due to enhanced scattering and carrier concentration changes. The relative variation $\Delta S/S_0$ follows a nonlinear dependence that can be satisfactorily approximated by a quadratic function of absorbed dose. However, at high temperatures $(T \geq 500-600\ K)$, the Seebeck coefficients of irradiated and non-irradiated samples converge, demonstrating strong radiation stability of thermoelectric properties in the intrinsic conduction regime.

Overall, Tb doping effectively tunes the electronic structure, carrier type, and thermoelectric response of $SnSe$ −based solid solutions, enabling controlled $p-n$ conversion and optimization of transport parameters in the intermediate temperature range. The demonstrated radiation stability at elevated temperatures further highlights the potential of $Tb_xSn_{1-x}Se$ materials for thermoelectric applications under irradiation environments.

ORCID

T.A. Jafarov, https://orcid.org/0009-0003-9069-7402; **O.M. Gasanov,** https://orcid.org/0000-0003-4888-7686;
Kh.A. Adgezalova, https://orcid.org/0009-0000-8966-4919; **I.M. Mammadov,** https://orcid.org/0009-0001-6039-6081;
J.I. Huseynov, https://orcid.org/0000-0002-4498-2400; **I.I. Abbasov,** https://orcid.org/0000-0001-8111-2642;
V.I. Haciyeva, https://orcid.org/0009-0003-6929-9602

REFERENCE

[1] J. Kim, O. Song, Y.S. Cho, M. Jung, D. Rhee, and J. Kang, "Revisiting Solution-Based Processing of van der Waals Layered Materials for Electronics," ACS Materials Au, **2**(4), 382–393 (2022). https://doi.org/10.1021/acsmaterialsau.2c00034

[2] I. Abbasov, M. Musayev, J. Huseynov, E. Gavrishuk, S. Asadullayeva, A. Rajabli, and D. Askerov, "Temperature behavior of X-Ray luminescence spectra of ZnSe," International Journal of Modern Physics B, **36**(02), 2250018 (2022). https://doi.org/10.1142/S0217979222500187

[3] R.S. Stepanov, P.I. Marland, and A.V. Kolobov, "Compositional and Structural Disorder in Two-Dimensional $A^{III}B^{VI}$ Materials," Crystals, **13**(8), 1209 (2023). https://doi.org/10.3390/cryst13081209

[4] J.I. Huseynov, M.I. Murguzov, and S.S. Ismayilov, "Specific features of self-compensation in $Er_xSn_{1-x}Se$ solid solutions," Semiconductors, **47**, 323–326 (2013). https://doi.org/10.1134/S106378261303010X

[5] I.I. Abbasov, M.A. Musayev, C.I. Huseynov, Q.Y. Eyyubov, N.N. Hasimova, A.J. Mammadova, A.A. Hadieva, *et al*., "A study of impurity defect photoluminescence in ZnSe:Cr and ZnSe:Fe in the near infrared at room temperature," Advanced Physical Research, **5**(3), 192-199 (2023).

[6] S.-D. Guo, and Y.-H. Wang, "Thermoelectric properties of orthorhombic group IV–VI monolayers from the first-principles calculations," J. Appl. Phys. **121**, 034302 (2017). https://doi.org/10.1063/1.4974200

[7] I.I. Abbasov, and J.I. Huseynov, "Charge-transfer processes in $(SnS)_{1-x}(PrS)_x$ Alloys," Ukrainian journal of physics, **62**(10), 883-888 (2017). http://jnas.nbuv.gov.ua/article/UJRN-0000795750

[8] S. Isber, and X. Gratens, "Crystal growth and magnetic properties of tin selenide-doped europium$Sn_{1-x}Eu_xSe$," Journal of Magnetism and Magnetic Materials, **322**, 1113–1116 (2010). https://doi.org/10.1016/j.jmmm.2009.09.015

[9] B. Wei, J. Zhang, L. Lin, T. Wu, Z. Cheng, Y. Ma, J. Li, and S. Yu, "Enhancing Electrical Transport Performance of Polycrystalline Tin Selenide by Doping Different Elements," Physica Status Solidi (A) Applications and Materials, **221**(9), 2300717 (2024). https://doi.org/10.1002/pssa.202300717

[10] X. Yang, X-Y. Ma, T.-E. Shi, W-Q. Bao, J. Wang, Z.-Y. Wang, Y.-X. Zhang, *et al*., "High thermoelectric properties in polycrystalline SnSe materials realized by rare earth halide Co-doping," Ceramics International, **50**(11 Part B), 20515-20524 (2024). https://doi.org/10.1016/j.ceramint.2024.03.173

[11] S. Li, L. Yin, Y. Liu, X. Wang, C. Chen, and Q. Zhang, "Rare earth element Ce enables high thermoelectric performance in n-type SnSe polycrystals," Journal of Materials Science & Technology, **143**, 234-241 (2023). https://doi.org/10.1016/j.jmst.2022.09.054

[12] B.M. Askerov, *Electron Transport Phenomena in Semiconductors*, (World Scientific, Singapore, New Jersey, London, 1994).

[13] R. Yamada, T. Nomoto, A. Miyake, T. Terakawa, A. Kikkawa, R. Arita, M, Tokunaga, *et al*., "Nernst Effect of High-Mobility Weyl Electrons in NdAlSi Enhanced by a Fermi Surface Nesting Instability," Physical Review X,**14**, 021012 (2024). https://doi.org/10.1103/PhysRevX.14.021012

[14] S. Akhanda, K.A. Schlaak, E.F. Scott, N.A. Taj, S.J. Watzman, and M. Zebarjadi, "Thermomagnetic responses of semimetals," J. Appl. Phys. **135**, 240901 (2024). https://doi.org/10.1063/5.0192824

[15] J.I. Huseynov, and T.A. Jafarov, "The Influence of γ-Irradiation on Thermoemf and Heat Conduction of $Ln_{0.01}Sn_{0.99}Se$ (*Ln* – *Pr, Tb,Er*) Monocrystals," World Journal of Condensed Matter Physics,**4**(1), 1-5 (2014). http://dx.doi.org/10.4236/wjcmp.2014.41001

[16] I.I. Aliev, J.I. Huseynov, M.I. Murguzov, Sh.S. Ismailov, and E.M. Gojaev, "Phase relations and properties of alloys in the SnSe-DySe system," Inorg. Mater. **50**, 237–240 (2014). https://doi.org/10.1134/S0020168514030029
[17] Sh.S. Ismailov, J.I. Huseynov, M.A. Musaev, I.I. Abbasov, and V.A. Abdurakhmanova, "Effect of doping level and compensation on thermal conductivity in $Ce_xSn_{1-x}Se$ solid solutions," Low Temp. Phys. **46**, 1114–1120 (2020). https://doi.org/10.1063/10.0002155
[18] I.I. Abbasov, Sh.S. Ismailov, J.I. Huseynov, V.A. Abdurakhmanova, "Concentration dependences of electrical conductivity and the Hall effect of the $Ce_xSn_{1-x}Se$ single crystals," Low Temp. Phys. **45**, 1277–1280 (2019). https://doi.org/10.1063/10.0000209
[19] J.I. Huseynov, Kh.A. Hasanov, T.A. Jafarov, and I.I. Abbasov, "Compensating effect of terbium impurity on the conductivity of $Tb_xSn_{1-x}Se$ solid solutions," Ukrainian journal of physics, **65**(3), 225-230 (2020). http://jnas.nbuv.gov.ua/article/UJRN-0001127989
[20] Sh.S. Ismailov, J.I. Huseynov, M.A. Musaev, I. I. Abbasov, and A. Abdurakhmanova, "Effect of doping level and compensation on thermal conductivity in $Ce_xSn_{1-x}Se$ solid solutions," Low Temperature Physics, **46**, 1114–1120 (2020). https://doi.org/10.1063/10.0002155
[21] T.A. Jafarov, O.M. Gasanov, Kh.A. Adgezalova, H.A. Aslanov, J.I. Huseynov, I.I. Abbasov, and R.Sh. Ragimov, "Modification of the kinetic parameters of *SnSe* by terbium doping," East Eur. J. Phys. (4), 407 (2025). https://doi.org/10.26565/2312-4334-2025-4-39
[22] J.I. Huseynov, M.I. Murguzov, S.S. Ismayilov, R.F. Mamedova, and E.M. Gojayev, "On the thermopower and thermomagnetic properties of $Er_xSn_{1-x}Se$ solid solutions," Semiconductors, **51**, 153–157 (2017); https://doi.org/10.1134/S1063782617020075
[23] J.I. Huseynov, and T.A. Jafarov, "Effect of γ-ray radiation on electrical properties of heat-treated $Tb_xSn_{1-x}Se$ single crystals," Semiconductors, **46**, 430–432 (2012). https://doi.org/10.1134/S1063782612040082
[24] M. Kockert, D. Kojda, R. Mitdank, A. Mogilatenko, Z. Wang, J. Ruhhammer, M. Kroener, *et al*.,"Nanometrology: Absolute Seebeck coefficient of individual silver nanowires," Sci. Rep. **9**, 20265 (2019). https://doi.org/10.1038/s41598-019-56602-9
[25] K.A. Hasanov, J.I. Huseynov, V.V. Dadashova, F.F. Aliyev, *et al.* "Effect of Phonon Drag on the Thermopower in a Parabolic QuantumWell," Semiconductors, **50**, 295–298 (2016). https://doi.org/10.1134/S106378261603009X
[26] S. Foster, and N. Neophytou, "Doping Optimization for the Power Factor of Bipolar Thermoelectric Materials," J. Electron. Mater. **48**, 1889–1895 (2019). https://doi.org/10.1007/s11664-018-06857-1
[27] D.I. Huseynov, M.I. Murguzov, and S.S. Ismailov, "Thermal conductivity of $Er_xSn_{1-x}Se$ ($x \leq 0.025$) solid solutions," Inorg. Mater. **44**, 467–469 (2008). https://doi.org/10.1134/S0020168508050063
[28] T. Rasmi, R.C. Bose, T.S. Varun, and K.A. Malini, "Impact of gamma irradiation on thermoelectric efficiency of Te-based thin films,"Radiation Physics and Chemistry, **242**, 113601 (2026). https://doi.org/10.1016/j.radphyschem.2026.113601
[29] J.I. Huseynov, M.I. Murquzov, and R.F. Mamedova, "Thermal Conductivity and Termal EMF of Materials for Thermal Energy Converters," in: *TPE-06 3rd Intern. Conf. on Technical and Physical Problems in Power Engineering*, (Ankara, 2008).
[30] V. Konye, and M. Oqata, "Thermoelectric transport coefficients of a Dirac electron gas in high magnetic fields," Phys. Rev. B, **100**, 155430 (2019). https://doi.orq/101103/PhysRevB.100.155430

ЗАМІЩУВАЛЬНА ВБУДОВА Tb, p-n ПЕРЕХІД ПРОВІДНОСТІ , ТА ВПЛИВ ГАММА-ОПРОМІНЕННЯ НА ТЕРМОЕЛЕКТРИЧНІ ВЛАСТИВОСТІ ТВЕРДИХ РОЗЧИНІВ $Tb_xSn_{1-x}Se$

Т.А. Джафаров[1], А.М. Аллахвердієв[1], Г.А. Гарашова[1], Х.А. Адгезалова[1], О.М. Гасанов[1], І.М. Мамедов[1], Дж.І. Гусейнов[1], І.І. Аббасов[2], В.І. Гаджиєва[3]

[1]Азербайджанський державний педагогічний університет, AZ-1000, Баку, вул. Уз. Гаджибейлі, 68, Азербайджан
[2]Азербайджанський державний університет нафти та промисловості, Az-1010, Баку, проспект Азадлик, 20, Азербайджан
[3]Нахчиванський державний університет, AZ7000, місто Нахчивань, вулиця Істіглал, 85, Азербайджан

Фізико-хімічні та термоелектричні властивості твердих розчинів $Tb_xSn_{1-x}Se$ ($0 \leq x \leq 0,05$) були систематично досліджені з акцентом на перехід типу носіїв, зумовлений складом, а також на ефекти γ-опромінення. Диференціальний термічний аналіз виявляє монотонне зниження температури плавлення та ентальпії зі збільшенням вмісту Tb, що вказує на спотворення кристалічної решітки та зниження термічної стабільності через заміщення Tb^{3+} на позиціях Sn^{2+}. Рентгенівська дифракція підтверджує однофазну орторомбічну (Pnma) структуру без вторинних фаз, тоді як EDX-аналіз підтверджує успішне включення Tb. Індукований складом p-n перехід відбувається у вузькому діапазоні концентрацій, що супроводжується значною зміною коефіцієнта Зеєбека. γ-опромінення (до 4-6,5 Мрад) суттєво впливає на коефіцієнт Зеєбека в області низьких температур (80-300 K) з нелінійною залежністю від дози, яку можна апроксимувати квадратичною функцією. За підвищених температур ($T \geq 500$ K) термоелектрична реакція демонструє значну радіаційну стабільність. Отримані результати чітко вказують на те, що легування Tb сприяє керованій модуляції властивостей транспорту носіїв заряду, зберігаючи при цьому структурну цілісність і термічну стабільність матеріалу за підвищених температур. Ці результати підкреслюють великий потенціал систем, легованих Tb, для передових термоелектричних застосувань, особливо в умовах експлуатації, що піддаються радіаційному впливу.

Ключові слова: *тверді розчини; замісне легування; p-n перехід провідності; коефіцієнт Зеєбека; гамма-опромінення; радіаційно-модифікований термоелектричний транспорт*